Supporting Text

Simulation Details. Simulations were carried out with the program CHARMM (1) using the PARAM27 force field with standard lipid (2), protein (3), and TIP3P water model (4) parameters. The use of particle-mesh Ewald (5), SHAKE (6), and constant pressure and temperature algorithms (7) in these simulations has been described elsewhere (8). The simulation system consists of a gramicidin A (gA) helical dimer [Protein Data Bank, PDB:1JNO (9)] embedded in a dimyristoylphosphatidylcholine (DMPC) bilayer (Fig. 1 of article), created using an extension of existing membrane-building techniques (10). The lipid bilayer contains 20 DMPC molecules, hydrated with 1 M KCl electrolyte solutions consisting of 19 K^+ and Cl^- pairs and 1080 water molecules. Hexagonal periodic boundaries, of side ∼31 Å and initial length ∼74 Å, were imposed on the protein-membrane system. The system was hydrated with a high electrolyte concentration to ensure good sampling of the bulk electrolyte and to help shield ions from periodic images.

During the simulations used to calculate the single-ion potential of mean force (PMF), $\mathcal{W}(\mathbf{r}_1)$, other ions were excluded from the sphere of radius 14 Å defining the pore region, using a repulsive flat-bottom spherical harmonic restraint with force constant 5 kcal/mol. To limit the lateral displacement of the ion, and thus insure good sampling in a well defined region of configurational space, we used a flat-bottom cylindrical restraint with radius 8 Å (relative to the center of mass of the dimer) and force constant 10 kcal/mol/Å^2. The side-chain of Trp 9 was maintained in the rotamer basin of PDB:1JNO (8) by imposing a flat-bottom harmonic potential with force constant 100 kcal/mol/rad^2.

For umbrella sampling calculations, harmonic potentials with force constant 10 kcal/mol/Å^2 were implemented for each of 101 windows, positioned in 0.5-Å increments from $-20 \leq z \leq +30$ Å. The initial configurations were selected from a 4-ns sample of unbiased molecular dynamics (MD) trajectory meeting the following criteria: correct Trp 9 rotameric state, a single ion inside 14 Å, and a continuous chain of water molecules inside the channel. When no configuration was found with a K^+ ion near the center of a window, a nearby water molecule was exchanged with the outermost ion. For each window, equilibration was carried out for 80 ps prior to 1 ns of trajectory generation for the PMF. The 101 simulations were carried out concurrently on different CPUs. The resulting biased ion density distribution was symmetrized by creating duplicate windows on opposite sides of the channel.

Ionic distributions were unbiased using the weighted histogram analysis method (WHAM) (11), with a bin size of 0.01 Å and a stringent tolerance of 0.001 kcal/mol on every point in the PMF (tested by comparing PMFs obtained 100 iterations apart to ensure good convergence). An additional four 1-ns simulations were generated without a window function to calculate the bulk limit $W_{\text{bulk}}(z,r) = -k_{\text{B}}T \ln\left(\langle\rho_{\text{bulk}}(z,r)\rangle / \overline{\rho}\right)$, where $\overline{\rho}$ is the K^+ density far from the channel ($30 < |z| < 35$ Å). $W_{\text{bulk}}(z,r)$ and $W(z,r)$ were matched in the range $25 < |z| < 29$ Å, for $r < 8$ Å, to set the correct bulk reference for the complete 2D PMF.

To confirm the barrier height in the 2D-PMF with free energy perturbation (FEP), a total of 11 windows with coupling parameter λ ranging from 0 to 1 was used in the FEP calculation, with the ion and water (and their hybrids) held at their z values with a harmonic force constant of 10 kcal/mol, and held on axis by a flat-bottom potential acting outside 0.5 Å with force constant 10 kcal/mol. WHAM was then used to give the total free energy change ΔG_{ex} for the perturbation (12). The local density of water at the center of the channel (at $z = 0$), calculated from an analysis of 80 ns of trajectory sampled with 0.5 and 1.0 Å side boxes, is 7.5-fold larger than in the bulk (at $z = 30$). The calculated free energy for exchanging an ion in the bulk with a water at the origin (ΔG_{ex} of Eq. 3 of article) was 9.8 ± 0.1 kcal/mol, whereas the increase in

water density inside the channel corresponds to 1.2 ± 0.3 kcal/mol, leading to an estimated free energy $\mathcal{W}(\mathbf{r}) - \mathcal{W}(\mathbf{r}')$ of 8.6 ± 0.4 kcal/mol that can be compared to that obtained from the 2D PMF.

Calculations of the charging free energy of a K^+ in a simple model single-file column of water used a model where a K^+ is fixed at the origin with four water molecules on each side held inside a cylindrical tube created by a flat-bottom harmonic potential of radius 0.25 Å and force constant 1000 kcal/mol/Å^2; planar restraints were placed at $z = \pm 12.5$ Å with force constant 100 kcal/mol/Å^2. The effect of a cavity reaction field arising from a continuum dielectric of 78.4 (corresponding to bulk water) outside a radius 15.3 Å was considered. The FEP calculations were carried out with the non-polarizable TIP3P water model (4) as well as the recently developed polarizable water model SWM4-DP (13) based on Drude oscillators. For all systems, the free energy for charging the K^+ was calculated using forward and backward FEP simulations, for a total of more than 2.2 ns.

To test the extent of the effect of polarizability of the phospholipid hydrocarbon tails on the stability of the ion, we carried out energy calculations on coordinates from a simulation of an enlarged fully atomic system with 96 DMPC molecules and a total of 24,037 atoms, following 1 ns of simulation with a K^+ ion held at the channel center ($z = 0$). The total energy of the nonpolarizable system was computed with particle mesh Ewald (PME) electrostatics with the ion at the center of the channel, relative to the bulk ($z = 20$ Å). This was then repeated with Drude oscillators on the carbon atoms of the lipid hydrocarbon chains, similar to the polarizable water simulations with the SWM4-DP water model. The polarizability for the carbon atom was set to 1.0 Å^3. The influence of induced polarizability was calculated according to a self-consistent field (SCF) procedure (i.e., by energy minimizing the position of the Drude oscillators while the real atoms are fixed). The change in the stabilization of the ion, due to lipid polarizability, was found to be -3.6 ± 0.3 kcal/mol. This result can be compared with the value obtained by raising the dielectric constant from 1 to 2 with Poisson solutions (-2.1 kcal/mol). This finding demonstrates that the continuum electrostatics approximation captures the effect of the polarizability but may underestimate its magnitude.

The Single-file Water Dipole and the Transmembrane Potential. The total PMF $W_{\rm tot}(z)$ used in the Nernst Planck equation of the paper can be expressed rigorously as a sum of the equilibrium PMF $W(z)$, dominated by local molecular interactions in the absence of any transmembrane potential, and the interaction of all atomic charges q_i, at positions z_i, in the pore region with the scalar potential $\phi_{\rm mp}$ arising from a very small ionic charge imbalance widely distributed at the membrane solution interface (14)

$$W_{\rm tot}(z) = W(z) - k_{\rm B}T \ln \left\langle e^{-\sum_i q_i \phi_{\rm mp}(z_i)/k_{\rm B}T} \right\rangle , \qquad [1]$$

where z is the location of the ion and the brackets represent an average over the equilibrium distribution. Following a cumulant expansion this becomes (14)

$$W_{\rm tot}(z) \approx W(z) + q_{\rm ion}\phi_{\rm mp}(z) + \langle \Delta\mu(z) \rangle \frac{d}{dz}\phi_{\rm mp} - \frac{1}{2k_{\rm B}T} \left\langle \Delta\mu^2(z) \right\rangle \left(\frac{d}{dz}\phi_{\rm mp} \right)^2 , \qquad [2]$$

where $\Delta\mu(z)$ is the deviation from the mean value of the dipole moment of the pore system as a function of the position of the ion. Thus, a conductance calculation is complicated by the coupling of the dipole to the membrane potential, with the linear term in $\Delta\mu(z)$ influencing the flow of ions and the quadratic term creating an additional barrier as a consequence of the bimodal nature of the dipole distribution in the bulk.

Poisson Boltzmann (PB) solutions, together with histograms of the dipole moment of the single-file water column (and assuming the protein dipole contribution is negligible as a first approximation), obtained from biased trajectories, are used to estimate these perturbations to the equilibrium PMF. The function $\phi_{\rm mp}$ is calculated from the modified PB equation (14), given by

$$\nabla \cdot [\epsilon(\mathbf{r})\, \nabla \phi_{\rm mp}(\mathbf{r})] - \bar{\kappa}^2(\mathbf{r})\, [\phi_{\rm mp}(\mathbf{r}) - V_{\rm mp} H(\mathbf{r})] = 0, \qquad [3]$$

where $\epsilon(\mathbf{r})$ is the space-dependent dielectric constant, $\bar{\kappa}(\mathbf{r})$ is the space-dependent Debye screening factor, $V_{\rm mp}$ is the potential difference applied across the membrane, $H(\mathbf{r})$ is a step-function that is 1 on one side of the membrane and 0 everywhere else. This equation is solved for an MD-averaged gA structure in a 25-Å membrane slab of dielectric constant 2, using 1 M KCl salt in the bulk regions with dielectric constant 80. The charge distribution within the pore region is represented by the expansion in the dipole moment, dominated by the single-file water column, in Eq. 2, and thus the dielectric constant is set to 1 inside the protein and channel regions.

Figure 5*A* shows the membrane potential term $q_{\rm ion}\phi_{\rm mp}$ of Eq. 2, increasing linearly across the channel. Figure 5*B* shows the first correction of Eq. 2 (due to the linear term in the dipole of the single file column), and Fig. 5C the second correction (due to the quadratic term in the dipole moment). For example, when 100 mV is applied across the membrane (solid curves in Fig. 5), the linear and quadratic dipole corrections are of maximum amplitude 0.15 and 0.04 kcal/mol, respectively. For an applied voltage of 250 mV (dashed curves) these corrections are of maximum amplitude 0.35 and 0.25 kcal/mol, respectively. Therefore, as the voltage applied across the membrane is increased, these corrections can have considerable effect on the conductance.

Ion Diffusion Profile. The space-dependent diffusion coefficient $D(z)$ is extracted from the Laplace transform of the velocity correlation function of the velocity, using an analysis based on the generalized Langevin equation for a harmonic oscillator. For each window simulation, we calculate the following function (15)

$$D(z) = \lim_{s\to 0} \frac{-\hat{C}(s;z)\, \langle \delta z^2 \rangle_{(i)}\, \langle \dot{z}^2 \rangle_{(i)}}{\hat{C}(s;z) \left[s\, \langle \delta z^2 \rangle_{(i)} + \langle \dot{z}^2 \rangle_{(i)} / s \right] - \langle \delta z^2 \rangle_{(i)}\, \langle \dot{z}^2 \rangle_{(i)}}, \qquad [4]$$

where $C(t;z)$ is the velocity autocorrelation function for the ion at position z, and $\hat{C}(s;z)$ is the Laplace transform of this function. To estimate the value of the limit as $s \to 0$, we linearly extrapolate from the range $15 \leq s \leq 35$. Figure 6 shows the axial ion diffusion coefficient of the ion as a function of its position.

Single Ion Dissociation Constant. The equilibrium single ion dissociation constant $K_{\rm D}$ can be expressed in terms of the three-dimensional single ion PMF, $\mathcal{W}(\mathbf{r})$, as (14)

$$K_{\rm D}^{-1} = \frac{\int d\mathbf{r}\, \mathcal{H}_{\rm site}(\mathbf{r})\, e^{-\mathcal{W}(\mathbf{r})/k_{\rm B}T}}{e^{-\mathcal{W}(\mathbf{r}')/k_{\rm B}T}}. \qquad [5]$$

where $\mathbf{r}'$ is a chosen reference ion position, $k_{\rm B}$ is the Boltzmann constant, T is the temperature and the binding site is defined by the Heaviside step function $\mathcal{H}_{\rm site}(\mathbf{r})$, which is 1 inside the binding site and 0 outside. $K_{\rm D}$ may also be expressed in terms of the 1D PMF, $W(z)$, which can be obtained by integrating over the allowed lateral displacements in xy-space. Because we impose a cylindrical restraint (a flat-bottom steep harmonic well of radius R) during simulations, such that the xy coordinates are always bounded, $W(z)$ is given by

$$e^{-W(z)/k_{\rm B}T} = C \int dx\, dy\, H_{\rm cyl}(x,y)\, e^{-\mathcal{W}(x,y,z)/k_{\rm B}T}, \qquad [6]$$

where C is a constant and

$$H_{\rm cyl}(x,y) = \begin{cases} 1; & \sqrt{x^2+y^2} \le R \\ 0; & \sqrt{x^2+y^2} > R \end{cases} . \quad [7]$$

We define the 1D PMF to be zero in the bulk at $z = 30$ Å, such that the constant C in Eq. 6 is

$$C = \frac{1}{\int dx\, dy\, H_{\rm cyl}(x,y)\, e^{-\mathcal{W}(x,y,30)/k_{\rm B}T}}. \quad [8]$$

Because $\mathcal{W}$ is independent of x and y at $z = 30$ Å, $\mathcal{W}(x,y,30) = \mathcal{W}(0,0,30)$ and thus

$$C = \frac{e^{+\mathcal{W}(0,0,30)/k_{\rm B}T}}{\pi R^2}. \quad [9]$$

which can be inserted into Eq.6 to give

$$e^{-W(z)/k_{\rm B}T} = \frac{1}{\pi R^2} \int dx\, dy\, H_{\rm cyl}(x,y)\, e^{-[\mathcal{W}(x,y,z)-\mathcal{W}(0,0,30)]/k_{\rm B}T}, \quad [10]$$

Now, if we define the binding site within the range $z_{\rm min} \le z \le z_{\rm max}$ in the axial direction

$$\mathcal{H}_{\rm site}(\mathbf{r}) = h_{\rm site}(z)\, H_{\rm cyl}(x,y), \quad [11]$$

where

$$h_{\rm site}(z) = \begin{cases} 1; & z_{\rm min} \le z \le z_{\rm max} \\ 0; & z < z_{\rm min} \\ 0; & z > z_{\rm max} \end{cases} , \quad [12]$$

then Eq.5 becomes

$$K_{\rm D}^{-1} = \int dx\, dy\, dz\, \mathcal{H}_{\rm site}(x,y,z)\, e^{-[\mathcal{W}(x,y,z)-\mathcal{W}(0,0,30)]/k_{\rm B}T} \quad [13]$$

$$= \int dz\, h_{\rm site}(z) \int dx\, dy\, H_{\rm cyl}(x,y)\, e^{-[\mathcal{W}(x,y,z)-\mathcal{W}(0,0,30)]/k_{\rm B}T}. \quad [14]$$

Using Eq. 10, the coefficient in front of the integral for $K_{\rm D}^{-1}$ becomes the accessible cross sectional area of the ion in the bulk region, equal to the area of the restraining cylinder πR^2, applied during simulations ($\pi 8^2 = 201$ Å^2)

$$K_{\rm D}^{-1} = \pi R^2 \int dz\, h_{\rm site}(z) e^{-W(z)/k_{\rm B}T} \quad [15]$$

$$= \pi R^2 \int_{z_{\rm min}}^{z_{\rm max}} dz\, e^{-W(z)/k_{\rm B}T}. \quad [16]$$

Two-dimensional Histograms and PMFs. Distributions, biased in z, involving some secondary variable s (such as solvation number or dipole moment of the single file water column), $\rho^{\rm bias}(z,s)$, may be unbiased to produce additional 2D PMFs $W(z,s)$. We obtained the conditional probability $\rho(s;z)$ (the probability of having variable s, given the ion is at position z) from the histogram of biased density. The unbiased distributions, which are related to the biased distributions via the WHAM equations, obey a similar relation and the 2D PMF becomes

$$W(z,s) = W(z) - k_{\rm B}T \ln \langle \rho(s;z) \rangle + C, \quad [17]$$

where C is a constant. Fig. 7 shows the 2D histogram of the ion hydration number (water oxygen atoms within 3.6 Å) as a function of coordinate z, from which the 2D PMF $W(z, n)$ shown in Fig. 3 was calculated. The ion is solvated by 6–7 waters in the bulk electrolyte, as is also seen in the 2D PMF $W(z, n)$. Dehydration occurs gradually as this number drops to just 2 inside the single-file column within the channel.

The 2D histogram $P(z, n)$ of Fig. 7 was formed for $|z|$ in 0.5 Å blocks and $0 \leq n \leq 10$, where n is the discrete number of water molecules residing within 3.6 Å of the K^+ ion. This distribution was then interpolated onto a 0.1 Å grid. Before calculation of the 2D PMF $W(z, n)$, the histogram $P(z, n)$ was symmetrized with respect to the origin $z = 0$, and smoothed with a Gaussian filter in the z direction only (with standard deviation 0.5 Å).

The distribution of the dipole moment of the single-file water molecules (Fig. 4A of the article), as a function of ion position z, was calculated by considering the net dipole of all water molecules inside a radius 14 Å sphere, with respect to the center of mass of the gA dimer. The histogram was calculated by interpolating onto a 0.1 Å grid, and discretizing dipole moments on a 1 D grid. Before calculation of the 2D PMF $W(z, \mu)$ (Fig. 4B of the article) the histogram $P(z, \mu)$ was antisymmetrized, with respect to the origin $z = 0$, and Gaussian smoothing was applied in the z direction only (with standard deviation 0.5 Å).

References

1. Brooks, B. R., Bruccoleri, R. E., Olafson, B. D., States, D. J., Swaminathan, S., & Karplus, M. (1983) *J. Comput. Chem.* **4**, 187–217.

2. Schlenkrich, M., Brickmann, J., MacKerell, A. J., & Karplus, M. (1996) in *Biological Membranes. A molecular perspective from computation and experiment*, eds. Merz, K. & Roux, B. (Birkhauser, Boston), pp. 31–81.

3. MacKerell-Jr, A. D., Bashford, D., Bellot, M., Dunbrack, R. L., Evanseck, J. D., Field, M. J., Fischer, S., Gao, J., Guo, H., Ha, S., Joseph-McCarthy, D., Kuchnir, L., Kuczera, K., Lau, F. T. K., Mattos, C., Michnick, S., Ngo, T., Nguyen, D. T., Prodhom, B., Reiher-III, W. E., Roux, B., Schlenkrich, B., Smith, J., Stote, R., Straub, J., Watanabe, M., Wiorkiewicz-Kuczera, J., & Karplus, M. (1998) *J. Phys. Chems. B* **102**, 3586–3616.

4. Jorgensen, W. L., Chandrasekhar, J., Madura, J. D., Impey, R. W., & Klein, M. L. (1983) *J. Chem. Phys.* **79**, 926–935.

5. Darden, T., York, D., & Pedersen, L. (1993) *J. Chem. Phys.* **98**, 10089–10092.

6. Ryckaert, J. P., Ciccotti, G., & Berendsen, H. J. C. (1977) *J. Comp. Chem.* **23**, 327–341.

7. Feller, S. E., Zhang, Y. H., Pastor, R. W., & Brooks, B. R. (1995) *Journal of Chemical Physics* **103**, 4613–4621.

8. Allen, T. W., Andersen, O. S., & Roux, B. (2003) *J. Am. Chem. Soc.* **125**, 9868–9877.

9. Townsley, L. E., Tucker, W. A., Sham, S., & Hinton, J. F. (2001) *Biochemistry* **40**, 11676–11686.

10. Woolf, T. & Roux, B. (1996) *PROT. Struc. Funct. Gen.* **24**, 92–114.

11. Kumar, S., Bouzida, D., Swendsen, R. H., Kollman, P. A., & Rosenberg, J. M. (1992) *J. Comp. Chem.* **13**, 1011–1021.

12. Souaille, M. & Roux, B. (2001) *Comp. Phys. Comm.*

13. Lamoureux, G., MacKerell, A. D., & Roux, B. (2003) *J. Chem. Phys.* **119**, 5185-5197.

14. Roux, B. (1999) *Biophysical Journal* **77**, 139–153.

15. Crouzy, S., Woolf, T., & Roux, B. (1994) *Biophys. J.* **67**, 1370–1386.

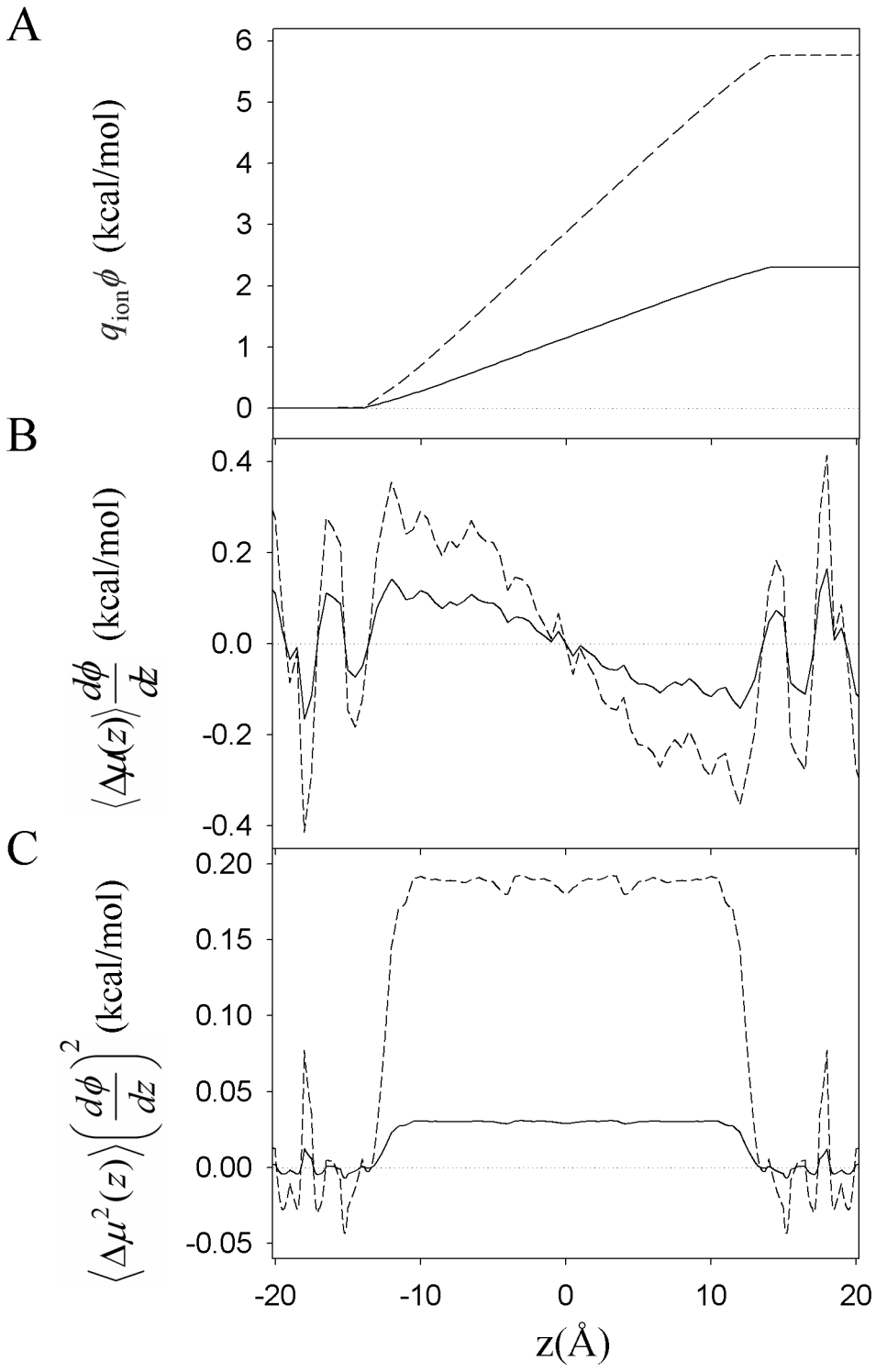

Fig. 5. Terms in the cumulant expansion Eq. 2. (A) The membrane potential. (B) The first, linear dipole correction. (C) The second, quadratic dipole correction. The solid curves are the results for 100 mV applied potential difference and the dashed curves are for 250 mV.

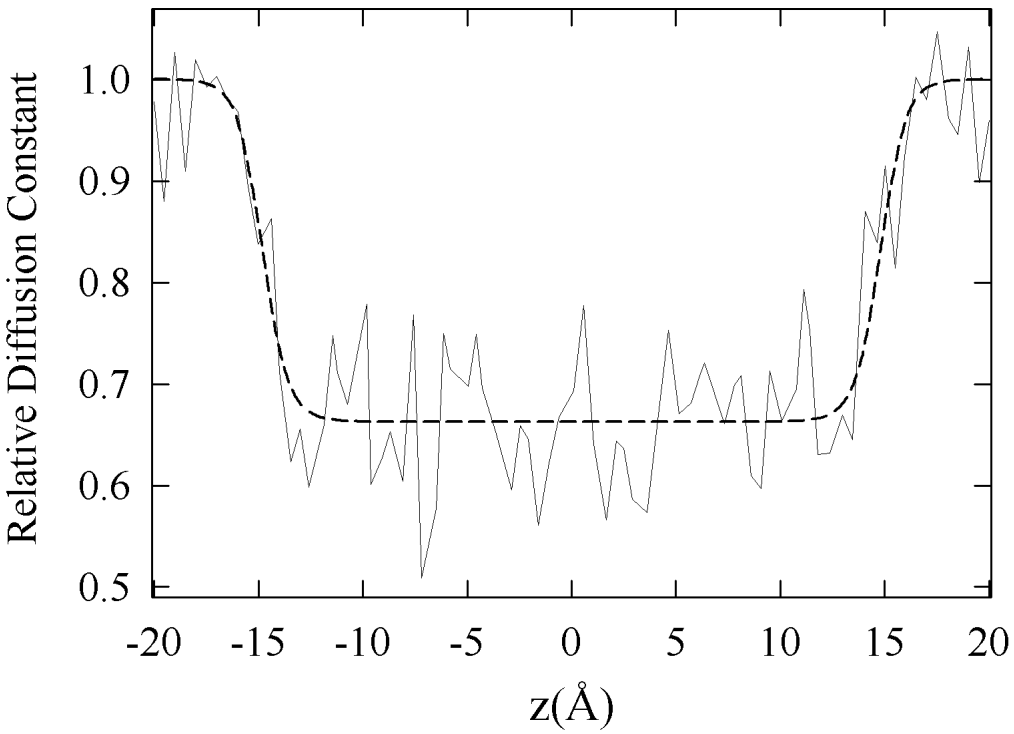

Fig. 6. K^+ ion diffusion profile. Calculated values of the axial component of the ion diffusion coefficient, for each window simulation, are drawn with a solid line. All values have been scaled relative to the calculated bulk value of 0.37 $Å^2$/ps. The fit (dashed line) is a symmetrized sigmoidal function.

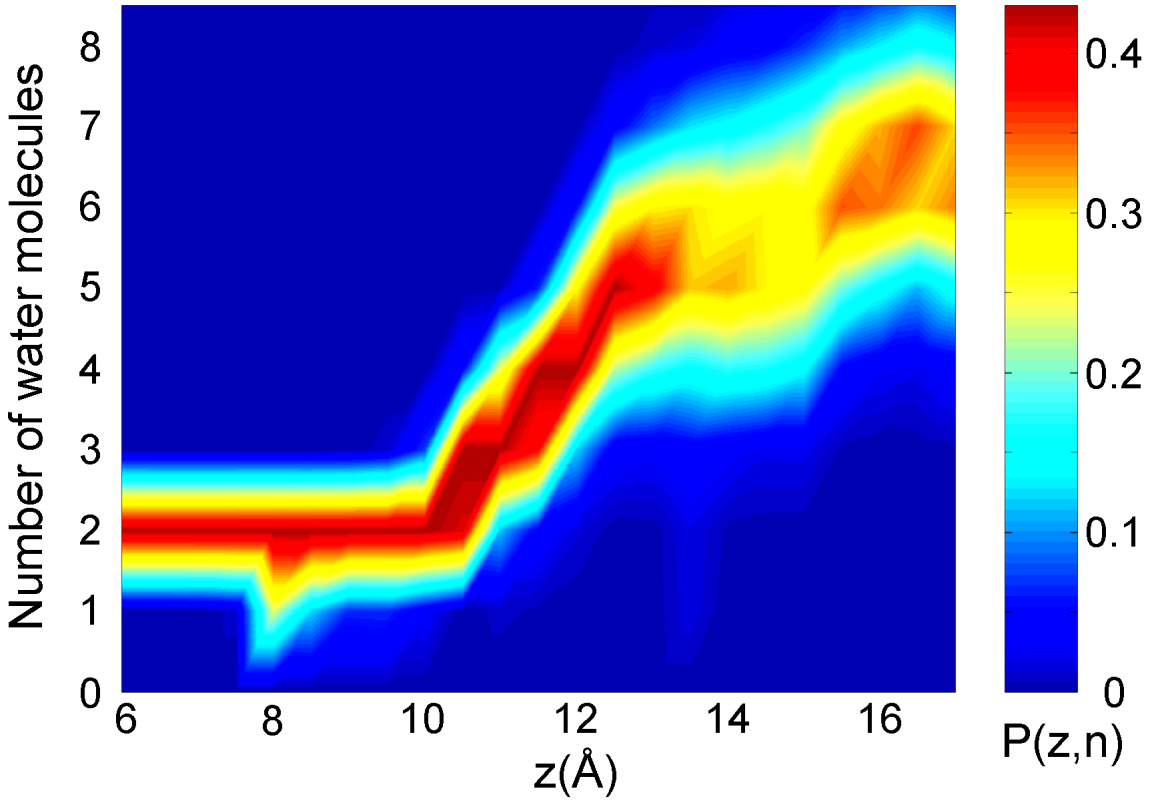

Fig. 7. Histogram of hydration number as a function of ion position z, corresponding to the 2D PMF $W(z, n)$ in Fig. 3.